PHARMACIA

Pharmacia 70(4): 1529–1540
DOI 10.3897/pharmacia.70.e114935

Research Article

Lead drug discovery from imidazolinone derivatives with *Aurora kinase* inhibitors

Bathula Sivakumar[1], Ilango Kaliappan[1]

1 *Department of Pharmaceutical Chemistry, SRM College of Pharmacy, SRM Institute of Science and Technology, Kattankulathur - 603203, Chengalpattu (Dt), Tamil Nadu, India*

Corresponding author: Ilango Kaliappan (ilangok67@gmail.com)

Received 30 October 2023 ♦ **Accepted** 9 November 2023 ♦ **Published** 18 December 2023

Citation: Sivakumar B, Kaliappan I (2023) Lead drug discovery from imidazolinone derivatives with *Aurora kinase* inhibitors. Pharmacia 70(4): 1529–1540. https://doi.org/10.3897/pharmacia.70.e114935

Abstract

Cancer is the second leading cause of death worldwide, and breast cancer accounts for 6.27 million cases in the year 2022. In the present study, Quantitative Structural Activity Relationship (QSAR) studies were performed on a dataset of 39 molecules of Imidazolinone analogues using in random selection using QSARINS Software. The statistically validated (R^2 = 0.8429 Q_{2loo} = 0.7558) MLR model was used to predict the bioactivity of novel leads. Moreover, high-scoring compounds were exposed to molecular docking and molecular dynamic modeling study. Intended derivatives 1–23 exhibited the anticipated bioactivity using a QSAR model. Aforementioned molecules were tested for binding affinities with the target protein and the majority of them demonstrated excellent interactions with binding pocket residues. Molecular dynamics simulations using Desmond for 100 ns of top complexes **1, 7, 9, 13** and **19** showed critical structural data concerning *Aurora kinase* inhibition. There were stable hydrophobic and hydrophilic interfaces in the dynamic site of compounds with a leading chemical structure. The chemical interacts to the (PDB: 1MQ4) structure in a stable way, according to RMSD, RMSF, RoG, H-bond, and SASA analysis. Furthermore, the docking results have been confirmed by MM-PBSA and MM-GBSA. Based on our findings, we reported the inclusion of the necessary structural features of imidazolinone derivatives leads to the development of the potent candidates for further development.

Keywords

Molecular descriptors, Molecular docking, Molecular dynamic study, QSAR

Introduction

Breast cancer is a leading reason for mortality among women of all ages. It replaces lung cancer as that of the second-leading reason for death in women. In 2022, the world's health organization (WHO 2022) predicted 6.27 million breast cancer-related deaths (Siegel et al. 2022). The prevalence of breast cancer is increasing worldwide at a dangerous rate. Annually, 2.5 million women are diagnosed with breast cancer, which in most postmenopausal women was issued by estrogen (Jia et al. 2022). In about 80% of patients, breast cancer is hormone-responsive (Chen et al. 2022). Due to the generation of estrogen in peripheral tissues, postmenopausal women have a higher chance of developing breast cancer than premenopausal women, whose primary source of estrogen production is the ovaries. Estrogen is crucial in encouraging the proliferation of cytotoxic breast epithelial cells in breast tumour patients with hopeful estrogenic receptors through signaling estrogen receptormediated alleyways. As a result, patients with breast cancer of the hormone-dependent kind have been found to have an increased risk of metastasis

and recurrence when their estrogen levels are high (Leino et al. 2022). The progression of hormone-dependent breast cancer can be prevented, managed and controlled using one of two basic approaches: binding estrogen receptors with receptor antagonists (ERAs, such as tamoxifen, or preventing the generation of estrogen with *Aurora kinase* inhibitors (AIs) (Khalifa 2021). Due to the absence of the estrogenic impact on the uterus and vasculature, it was discovered that AIs had fewer side effects than estrogen receptor antagonists. Two major categories of *Aurora kinase* inhibitors can be distinguished based on their work. Type 1 comprises steroidal AIs like exemestane and formestane which permanently suppress the activity of the *Aurora kinase* enzyme. Barasertib, Alisertib and Danusertib are examples of the second group of nonsteroidal AIs, which inhibit the activity of the *Aurora kinase* and have reversible inhibitory effects (McEwan 2021).The AIs showed significant outcomes in breast cancer treatment when compared to target estrogen receptor modulators for postmenopausal females with positive estrogen receptors treated with Tamoxifen, Arimidex alone or combined (ATAC) trials (Chumsri et al. 2011). Even though available AIs, whether steroidal or nonsteroidal, demonstrated positive clinical outcomes, prolonged use of them can result in the development of drug resistance and serious antagonistic properties, such as osteoporosis, cardiac disease, fragmented skeletons, and musculoskeletal and joint pain. Therefore, research into novel AIs is still necessary to develop substitute medications with better qualities (Karahalil et al. 2019).

Aminothiazoles were found to be used as starting materials for synthesizing the sulpha drugs, fungicides, dyes and biocides, as a thyroid inhibitor used in the treatment of hyperthyroidism and also to have antibacterial activity. Recent studies have proven that aminothiazoles are also used in the treatment of prion diseases. *Aurora kinases* are threonine/*serine kinases* that play a crucial role in cell division. They aid in the dispensation of genetic material from growing cells to their daughter cells (Hehnly et al. 2015). They perform a critical function in cellular division by controlling chromosomal segregation. Defects in this segregation produce genetic instability, a condition that is strongly linked to tumorigenesis. The first aurora kinases were discovered in Drosophila melanogaster, where mutations caused centrosome separation to fail, resulting in monopolar spindles resembling the northpole, hence the term aurora (Jung et al. 2006).

Experimental section

"QSARINS" enables the creation of numerous linear regression models using ordinary least squares, which are meticulously tested and validated using the chemometric technique. A series of amino thiazole derivatives with *Aurora kinase* inhibitory properties were selected from a 39-compound dataset (Suppl. material 1: table S1) published in the literature. The pIC_{50} values were transformed and used as a dependent variable.

The data collection, integration, curation, model creation, and model validation procedures are all included in the QSAR modelling study. Using an associated algorithm, a thorough analysis of the collected molecular descriptors yielded structure and bioactivity relationships. In our situation, atomic charges, Sanderson's electronegativity, MoRSE descriptors, as well as 3D structural approximations constructed on electron diversion descriptors biased by volume, all played a significant part in predicting bioactivity (Gramatica 2020). When molecular descriptors are weighted, the molecules become delicate to the occurrence of specific components on them. The polarizability and ionizability weighing terms, in particular, were influenced by the scattering parameter's volatility at bigger terms, often beyond the target value of 26. The reported QSAR model shown below does not exhibit significant value volatility in repeated testing. The enduring standards formed by the erected QSAR model indicate that the bioactivity deviation since the investigational reserve assessment was not significant. The preferred QSAR model, which delivered mechanical evidence, assisted in the improvement of authoritative drugs with enhanced Aurora kinase inhibitory action (Adawara et al. 2020).

Molecular alignment and conformer creation in compound design

Based on our study on the interactions between the hydrophobic and hydrophilic areas of the Brest cancer active site provided us with significant information for developing inhibitors. Table 1 shows the geometry optimisation and Avogadro tool results for the 23 suggested compounds with varied heterocyclic rings, functional groups, and 2-amino thiazole chain linkers. During the docking research, the best short energy conformers for each ligand that could be discovered were chosen.

Molecular docking

The aforementioned conformations were imperilled to *Insilco* experiments in order to investigate the interactions between residues, H-bonds, and obligatory energy scores. The novel Aurora kinase pattern, PDB 3D structures: 1MQ4, was produced from the protein catalogue (www.rcsb.org) (Behera et al. 2021). Missing residues were restored using the Modeller V 9.23 program19 after hydrogen atoms were added and pre-existing ligands were removed. The cocrystallized ligand was re docked to 1MQ4 active sites to determine the docking restrictions. Proteins were created through the addition of polar hydrogens in line with Kollman's unified atomic charges. The PDB fixer tool20 was used to analyse the histidine protonation residue states by assigning ND1 to zinc-bound histidines and NE2 to residual histidines.

The ligand categorizer was constructed by accumulating polar hydrogens and employing Gasteiger charges. The Auto grid selection allows users to generate the energetic map using a distance-dependent dielectric continuous utility by identifying an active site and setting the element size to 60 * 60 * 60 points with 0.503 A^0 spacing. The RMSD scores between the reference and predicted components were used to assess whether the docking simulation properly foretold a close-match docked pose or not (Rosário-Ferreira et al. 2021).

Simulations of molecular dynamics

The "Desmond V 5.9 software" was used to conduct simulations of molecular dynamics in order to investigate how the solvent system altered the molecular makeup of the proteinligand complex (Schrodinger 2019-3). The OPLS 4 force field was used for the docked complex's MDS (ligand 1MQ4). For the sake of performing dynamic forces simulations, the complex's site has been center filled in an orthorhombic cubic punnet, and TIP3P water molecules and buffers have been inserted at a distance of 10 A^0 between the box edge and the protein atom (Siva Kumar et al. 2022). The complex type boundary condition box volume has also been estimated, as have counter ions such as Na+ and Cl- that were inserted to randomly neutralise the system. A clinically tested 2-amino thiazole substituted imidazolidinone derivative was used as the reference chemical for comparing simulation results. The anticipated lead complex molecule 1MQ4 has 458 000 A^0 box volume and 28 252 atoms with 8124 waters for MD simulations. The complex is made up of over 49998 atoms and 9209 fluids. The Desmond procedure was used to diminish the solvated built system before relaxing using the OPLS 4 force field parameters. To keep heavy atoms on the solute in check, the system was simulated using the Berendsen NVT ensemble at a temperature of 10 K. The MDS was performed using the isothermal isobaric ensemble (NPT) at 300 K, 1 atom, and a thermostat relaxation time of 200 ps (NPT).

Using the Nose-Hoover thermostat and Martyne-Tobias-Klein barostat practices, the temperature and compression balances were kept at 300 K and 1 atom, respectively. Every 50 ps, the simulation progress were methodically recorded. Succeeding the replication phase, which needs 100 ns of manufacturing, the NPT ensemble was initiated. The simulated interaction diagram was utilised to investigate the trajectories of the frames, which assisted in the discovery of variations (Khetmalis et al. 2022).

Results and discussion

Intended novel derivatives Founded on absolutely correlated with structurally and molecular descriptor information from the QSAR model pIC_{50} = 5.1811+0.0168*(EstateVSA5)+0.0043*(PSA)+0.7620*(MoRSEP3)+1.3270*(MATSp 5)+12.5951*(RDFC24).

Fitting criteria

n_{tr} = 39 n_{pred} = R^2 = 0.8429 R^2adj = 0.7061 R^2-R^2adj = 0.0367 LOF = 0.0541 K_{xx} = 0.3885 $Delta_K$ = 0.0714 $RMSE_{tr}$ = 0.1762 MAE_{tr} = 0.1433 RSS_{tr} = 1.0241 CCC_{tr} = 0.8525 s = 0.1912 F = 20.2223

Internal validation criteria

Q_{2loo} = 0.7558 R^2-Q_{2loo} = 0.1101 $RMSE_{cv}$ = 0.2105 MAE_{cv} = 0.1702 $PRESS_{cv}$ = 1.4625 CCC_{cv} = 0.7954 Q_{2LMO} = 0.6076 R_{2Yscr} = 0.1289 Q_{2Yscr} = -0.2219 $RMSE_{AVYscr}$ = 0.3239 $RMSE_{ext}$ = 0.3697

External validation criteria

MAE_{ext} = 0.3167 $PRESS_{ext}$ = 0.8199 R^2_{ext} = 0.6726 $Q_{2\text{-}F1}$ = -0.2977 $Q_{2\text{-}F2}$ = -0.3627 $Q_{2\text{-}F3}$ = -0.1322 CCC_{ext} = 0.6877 $r^2_{m\ aver}$ = 0.2370 $r^2_{m\ delta}$ = 0.4976

Using alkyl linkers on imidazolidinone and a 2-amino thiazole ring on the tail, the 2-amino thiazole imidazolidin-4-one core structure was investigated. ESI the dataset chemicals used to create the QSAR models are shown in Table 1 along with the best leads discovered. Twentythree generated compounds were exposed to the descriptor deviousness tools of Chem DesChemoPy services using the lead structure as a template to determine the appropriate EstateVSA5, PSA, MoRSEP3, MATSp5, and RDFC24 values (Fig. 3). In most cases, the MoRSE descriptors (molecular representation of structure by electron diffraction) included weights for volume, atomic charges, Sanderson's electronegativity, and other variables in addition to the scattering parameter, which ranged from 1 to 23. (Table 1) displays the molecular descriptor values and structural details of 23 of the best-designed compounds along with estimates of their projected bioactivity at nano and sub-nano molar scales.

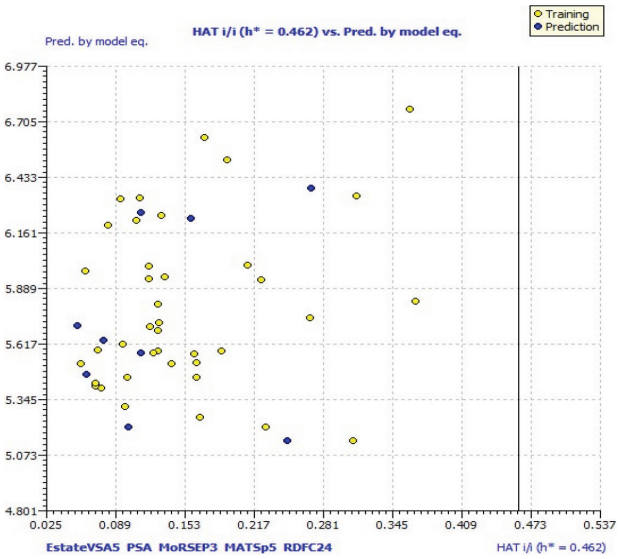

Figure 1. text, text, text.

Applicability domain. Hat diagonal values versus standardized residuals.

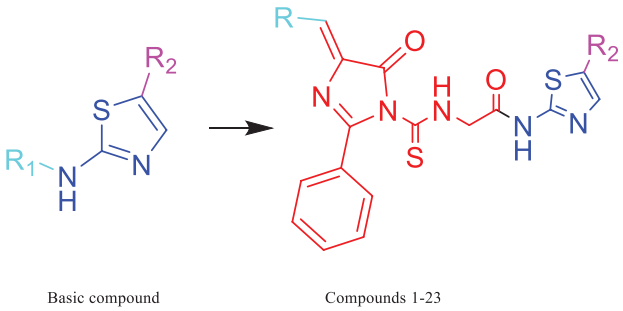

Figure 2. text, text, text.

Table 1. Molecular descriptor principles and predicted pic_{50} value for the 23 designed derivatives.

Name	EstateVSA5	PSA	MoRSEP3	MATSp5	RDFC24	Pred.Pki
1	23.71	222.071	-0.401	-0.107	0.052	6.7417275
2	35.852	252.400	-0.688	-0.150	-0.122	6.4286278
3	17.663	147.655	-0.427	-0.144	0.063	7.81143
4	23.719	259.48	0.008	-0.144	0.176	7.6593774
5	35.852	125.67	-0.400	-0.132	0.026	7.3411652
6	44.005	275.522	-0.154	-0.142	-0.015	6.349563
7	11.587	126.812	-1.452	-0.097	0.004	6.242778
8	30.829	268.487	-0.067	-0.146	0.048	5.740689
9	23.719	196.07	-2.188	-0.146	0.175	5.764796
10	47.975	233.577	-1.053	-0.135	-0.139	5.505607
11	41.909	241.284	-0.595	-0.156	-0.022	5.763515
12	11.587	259.962	0.070	-0.15	-0.024	5.849557
13	23.719	133.707	-0.757	-0.151	-0.194	5.978507
14	11.577	167.313	-1.129	-0.107	-0.006	5.846769
15	11.587	126.587	-1.545	-0.097	0.073	6.421773
16	47.975	154.355	0.382	-0.097	-0.069	6.283066
17	35.852	153.268	-0.558	-0.142	-0.061	6.257293
18	29.786	145.244	-1.45	-0.122	-0.013	6.720173
19	29.786	199.690	-0.296	-0.146	0.126	7.883326
20	11.587	128.361	-0.751	-0.136	0.102	5.816033
21	11.587	200.986	-0.037	-0.145	-0.193	6.191462
22	29.776	151.861	-1.570	-0.139	0.017	6.373608
23	35.842	152.813	-1.119	-0.042	0.012	5.653782

Molecular docking studies

The calculated novel derivatives with greatest pIC_{50} standards remained exposed to molecular docking studies for necessary empathy and H-bond interfaces estimate. Molecular docking was performed to investigate the potentiality of the chosen compounds, to engage the active cavity of *Aurora Kinase* in a way that would disrupt its tumorigenic activity. Many poses were observed and the poses with least score for each compound were considered. Interestingly, all the selected compounds except **2, 3, 10, 11, 12, 15** and **17** showed good interaction with the target in terms of glide score and energy; in particular than the reference compounds Tamoxifen and Arimidex. Results of the binding scores and the interactions with the amino acid residues are shown in Table 2. The active site pocket lies within the kinase domain of the target protein, which is essential for its function. Compound **19** having imidazolidionone and sulfonyl groups showed a least glide

Table 2. Amino acid interactions and docking scores ligand and significantly scored compounds.

Compound Code	Docking score (kcal/mol)	Glide energy (Kcal/mol)	H-bond interactions (distance in A^0)
1	-7.812	-126.364	LYS 143–1.96 LYS 162–2.27 ASN 261–2.48 ASP 274–2.01
2	-3.551	-136.422	LYS 143–2.17 LYS 162–2.26 ALA 213–2.18 ASN 261–2.67 ASP 274–2.33
3	-4.178	-121.158	ASP 256–1.93 ASN 261–1.92
4	-7.505	-128.895	LYS 143–2.76 ALA 213–1.99 LYS 258–2.42 ASN 261–2.15 ASP 274–1.70
5	-6.567	-113.935	LYS 143–2.05 LYS 258–3.34
6	-6.282	-129.258	ASN 261–2.11 ASP 274–2.26
7	-7.653	-130.38	LYS 143–1.83 LYS 162–2.04 ASN 261–2.51 ASP 274–1.88
8	-6.677	-131.410	LYS 162–2.01 ALA 213–2.28 LYS 258–2.24 ASN 261–1.97 ASP 274–1.97
9	-7.894	-123.094	LYS 162–1.69 ALA 213–2.09 LYS 258–2.50 ASN 261–2.11 ASP 274–2.03
10	-3.030	-130.443	LYS 162–2.34 ASN 261–2.22 ASP 274–1.71
11	-4.178	-121.158	LYS 143–2.07 LYS 162–2.23
12	-3.449	-122.071	LYS 143–2.29 LYS 162–2.34 ASP 274–2.03
13	-7.606	-127.369	LYS 143–1.69 ASN 261–2.33 ASP 274–1.80
14	-6.680	-132.345	LYS 143–2.32 LYS 162–2.18 ASN 261–2.70 ASP 274–2.74
15	-3.822	-129.061	LYS 143–2.32 LYS 162–2.19 ASN 261–2.55 ASP 274–1.94
16	-6.534	-119.101	LYS 143–2.19 ASN 261–2.23
17	-4.877	-126.472	LYS 143–2.58 LYS 162–1.94
18	-6.044	-126.472	LYS 143–2.01 LYS 162–2.24
19	-9.484	-130.410	LYS 162-1.98 GLU 211–2.19 ALA213–2.27 LYS 258–2.38 ASN 261–1.98

Compound Code	Docking score (kcal/mol)	Glide energy (Kcal/mol)	H-bond interactions (distance in A^0)
20	-6.545	-136.410	LYS 143–1.91
			LYS 162–1.91
			ASN 261–2.24
			ASP 274–1.87
21	-6.523	-124.212	LYS 143–2.17
			LYS 162–2.13
			ASP 274–1.98
22	-7.006	-124.475	LYS 143–2.00
			LYS 162–2.02
			ASN 261–2.24
			ASP 274–1.90
23	-7.520	-124.332	LYS 143–2.08
			ASN 261–2.38
			ASP 274–2.00
Tamoxifen	-5.003	-52.219	LYS 107–2.31
			ASP 108–2.42

score of -9.488KJ/mol^{-1} with the formation of five hydrogen bonds. The hydroxyl benzene group of compound **19** fits perfectly into the hydrophobic core of the active site sharing two hydrogen bonds with the residues Glu211 and Ala213. The core thiazole group shared two hydrogen bonds with Asp274 and Lys258 respectively. Moreover, an attractive non covalent pi-pi interaction was observed between the core group and Trp277 of the target. Compound **9** with substituted Aromatic P- Hydroxy benzaldehyde interacted through five hydrogen bonds with the binding site residues of the target *Aurora Kinase* possessing a docking score of -7.894KJ/mol^{-1}. It was noted that the bromo and hydroxy phenyl groups of both the compounds (Compound **19** and **9**) are located deeply inside the hydrophobic core due to their hydrophobic nature.

The superlative conformation of Derivatives **7**- 1MQ4 multifaceted from Glide demonstrated obligatory empathy as -7.653KJ/mol^{-1}. The sulfonyl and oxo groups of the compound showed interactions with the residues Lys143, Lys162, Asn261 and Asp274 through hydrogen bonding. Compared to the previous two compounds, this occupied different binding mode in the active pocket. The core thiazole imidazolidinone group shared four hydrogen bonds with the residues Lys143, Lys162, Asn261 and Asp274. In addition, a pi-pi interaction with the residue Trp277 was observed. Compound **1** shared five hydrogen bonds with the residues Lys162, Lys258, Asn261, Glu211 and Ala213. The thiazole group of the core component and the carbonyl sulphide of R1 shared hydrogen bonds with a single residue Lys 162. Interestingly, compound **19, 9** and **1, 7** showed similar binding modes respectively.

The best conformation of compound **13** - 1MQ4 complex from Glide displayed binding affinity as -7.520KJ/mol^{-1}. Similar to compound 1, the thiazole group of the core component and the carbonyl sulphide of R1 shared hydrogen bonds with a single residue Lys 162. Apart from that the residues Asp274, Asn261 and Lys143 were found to have H-bonded interactions. Compound **23** also showed good interaction with a docking score of -7.520 KJ/mol. Four hydrogen bonds involving the residues Asn261, Asp274 and Lys143 were observed with Asp274 forming two hydrogen bonds.

The compound **4** with substituted Aromatic cinnamaldehyde interacted with ALA 213 and

Oxo amino group interact with LYS 143, ASN 261 and ASP274 by the hydrogen bonding. The compound 22 with amino thiazole group moiety interacted with LYS 162, ASP 274 and Oxo and amino group interacted LYS 143, ASN 261, via H-bond. Bromo benzene formed pi-pi interactions with Trp277. Also it is evident from the table and figures, that all the above mentioned compounds showed better binding affinity than the control drug Tamoxifen. In addition, compounds **14, 8, 5, 20, 16, 21, 6** and **18** also showed good binding affinity than tamoxifen as evident from (Table 2) and their interaction are shown in Suppl. material 1: fig. S1.

Molecular dynamics simulation studies

Although molecular docking analyses have revealed the complex binding mechanisms (protein-inhibitor), molecular dynamics simulation can detect even the slightest disagreement. To find out as much as possible about the atomic specifics in the solvent system, the compounds **1, 7, 9, 13,** and **19** with the best interactions and energy docked conformation were studied (Fig. 3). For the MDS investigation, the active conformation with the best H-bond interactions, docking score and energy values were taken into account. We further looked into the simulation after a 100 ns simulation was run to determine the stability of the protein-inhibitor combination. Several parameters such as RMSD and RMSF of the protein and ligand, their respective torsion profiles and the histogram representing the ligand-protein

To study the stability of the bound complexes, the RMSD and RMSF calculations were performed. RMSD reflects the mobility of an atom during the MD simulation trajectory; with higher RMSD corresponding to higher mobility, whereas, lower RMSD corresponds to lower mobility. The RMSD plot indicates that the compounds **19, 9** and **7** stabilized shortly after commencing the simulation and found no major deviations throughout the simulation. Also a similar pattern of fluctuation was observed for both protein and ligand except for compound **13**. For compound **19**, the ligand RMSD varied from 0.91 to 2.48Å, whereas protein RMSD showed variation from 1.20Å to 2.19Å (Fig. 4). There was a small increase and decrease in RMSD of the protein and compound 19 respectively around 40–45 ns of simulation time. An initial drift was observed till 30 ns for compound **1**, after which certain stabilization could be observed. In case of Compound **9**-AurK complex, the protein showed a small decrease in RMSD between 48–51, suggesting minor conformational changes in the protein Compound **13** showed an increase in RMSD till 60 ns and started stabilizing further, whereas the protein undergone minor conformational change initially which might be due the flexibility of the residues. Moreover, compound 19 and compound 1 showed minimal deviation than the control drug tamoxifen.

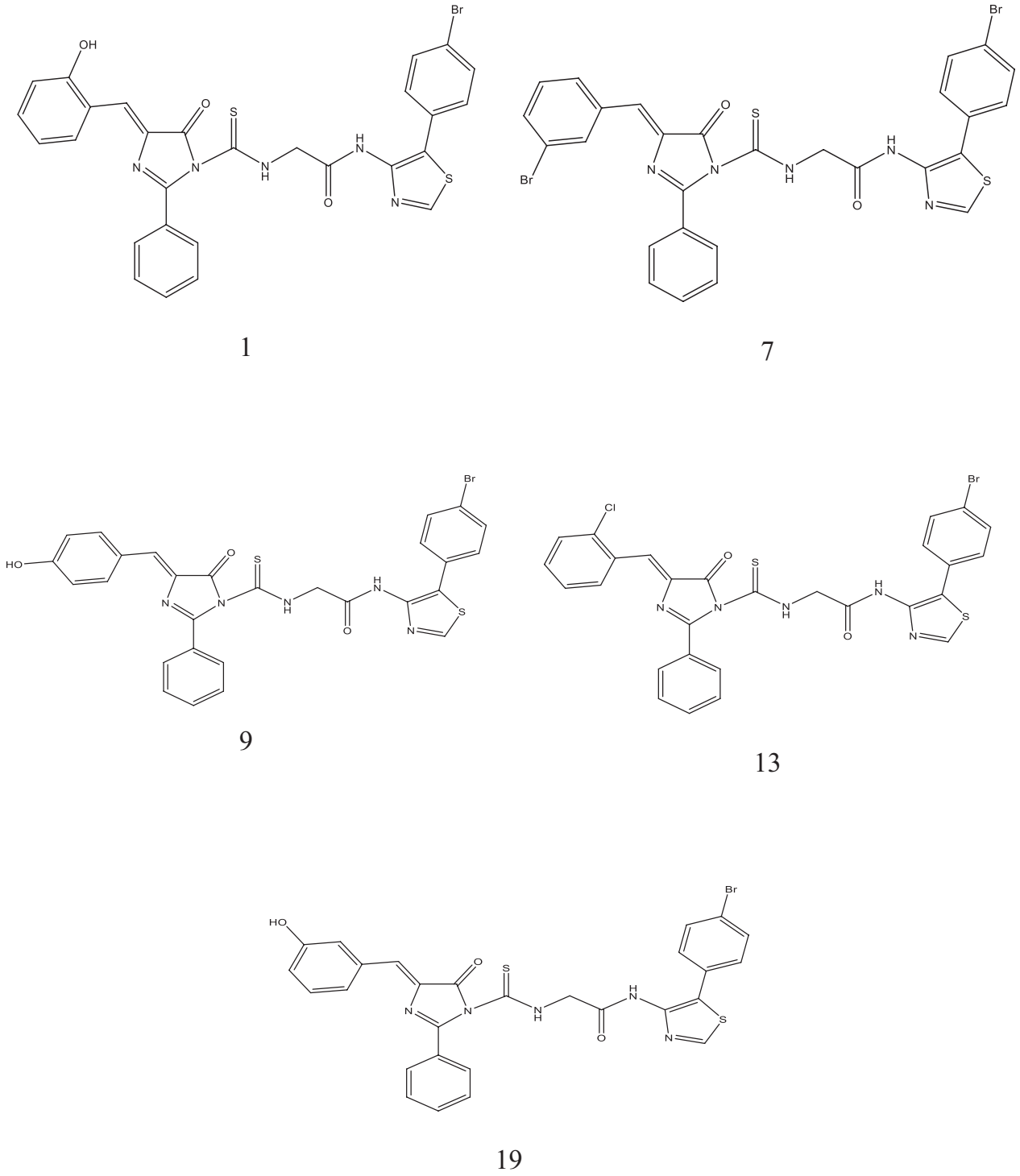

Figure 3. Leads generated from QSAR and docking studies (compounds 1, 7, 9, 13, 19) structural stability analysis upon ligand docking.

Gly173 is fluctuated to around 2.70 Å upon binding of Compound **19**. Secondary structural analyses showed a loop to stand conversion around the 180th residue, induced by compound 19. In case of Compound**1**-AurK complex, fluctuations were observed in regions of Thr287 to Gly291. From the ligand RMSF graph, the carbonyl and the thiazole groups of compound **19** are exposed towards the surface, which is also evident from the 2D plot (from docking). The benzyl group of compound 1 showed higher fluctuations than the other regions, suggesting their exposure to the surface. The residues Thr287 and Thr288 have fluctuated a bit upon binding of compound **7**. Notably, these fluctuations lie under the permissible range of 1–3Å. No major residual fluctuations were observed in Compound **9**-AurK complex. However, of the residues GLY 142, LYS 143, PHE 144, Glu 170, LYS 171 and ALA 172 showed an increase in flexibility (>3Å) interaction with compound **13**. Ligand RMSF (Fig. 5) also confirmed the exposure of the bromo-benzyl group towards the surface as evidenced from the 2D molecular docking interaction (Fig. 7).

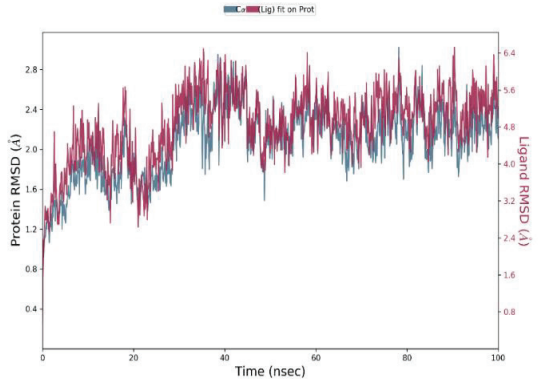

RMSD graph of Compound 1

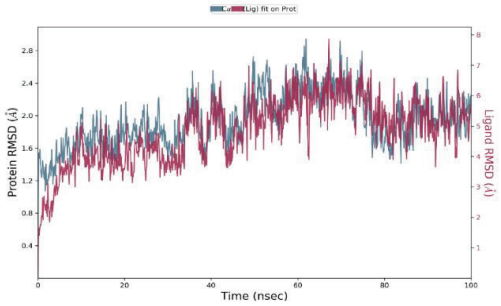

RMSD graph of Compound 7

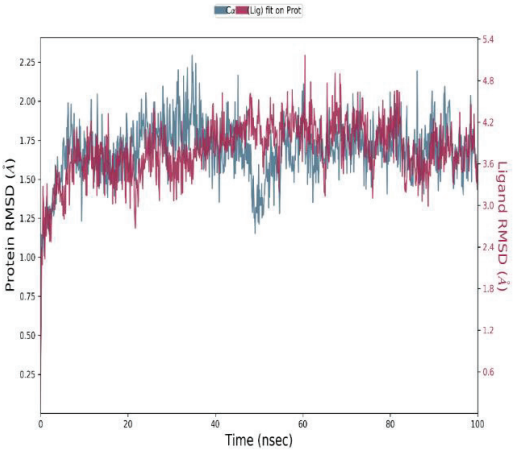

RMSD graph of Compound 9

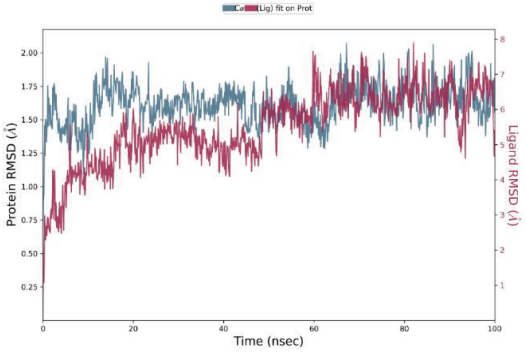

RMSD graph of Compound 13

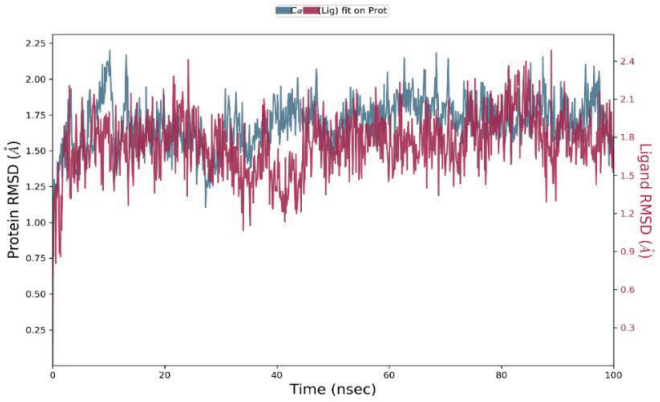

RMSD graph of Compound 19

Figure 4. The root mean square deviation (RMSD) of 1MQ4 protein during 100 ns MD, Compounds 1, 7, 9, 13, 19.

Preservation of intermolecular contacts in MDS

Interactions histogram showed the interactions lasting over different simulation time and the connections that past additional than 30% of the simulation time are measured. It shows that most of the interactions of the docked pose were retained during simulation. Water-bridge, Hydrogen bonding following hydrophobic interactions at stable areas LEU 139, GLY 142, LYS 143,

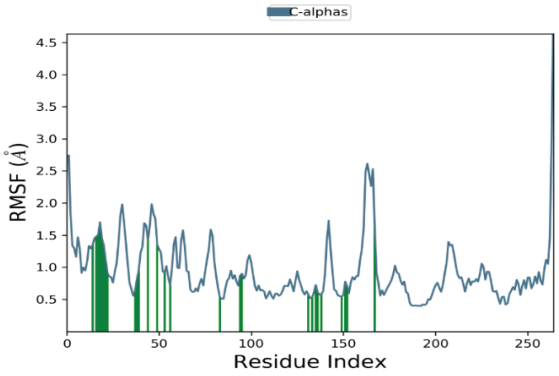

RMSF graph of Compound 1

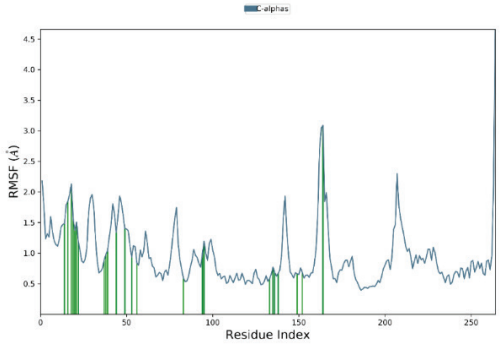

RMSF graph of Compound 7

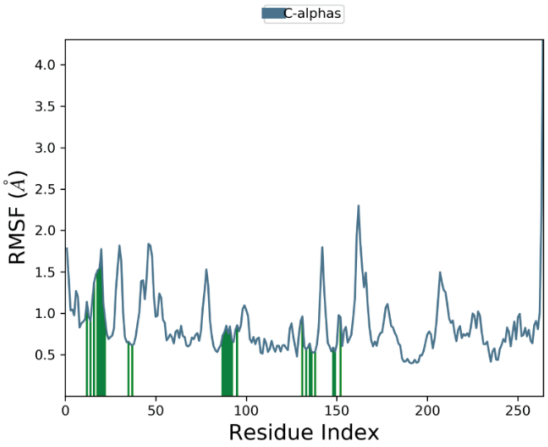

RMSF graph of Compound 9

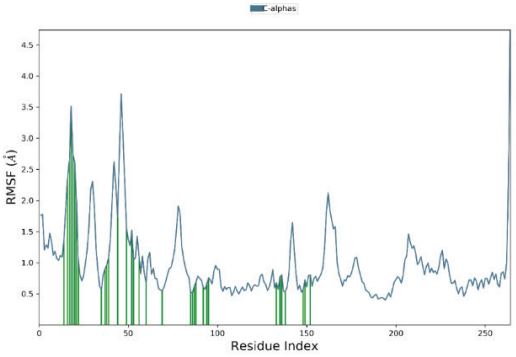

RMSF graph of Compound 13

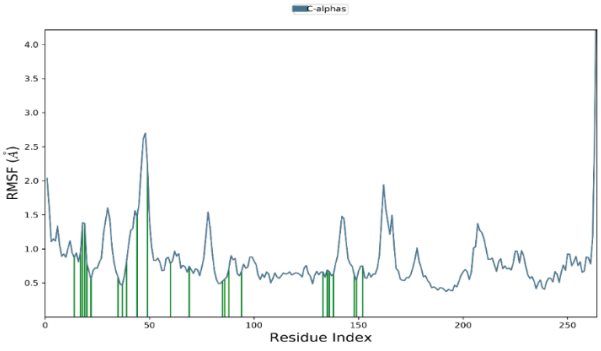

RMSF graph of Compound 19

Figure 5. The root mean square fluctuation (RMSF) of 1MQ4 protein during 100 ns MD, representing local changes along the protein chain for Compounds 1, 7, 9, 13, 19.

PHE 144, GLY 145, VAL 147, ALA 160, LYS 162, LYS 162, LEU 164, GLU 211, ALA 213, LYS 258, GLU 260, ASN 261, LEU 263, ASP 274 and TRP 277 were found in compound **19** during MDS (Fig. 6). Hydrogen bonds shared by the residues GLU 211, ALA 213, LYS162, ASN 261 and ASP 274 were retained. In addition, an aromatic amino acid PHE144 interacts with the keto group of the compound for 41% of simulation time. Compound **1** showed an additional hydrogen bond with LYS 162 and it was found that the compound was capable to interact retain interaction with the lysine residues compared to other interactions. Similar to Compound 1, compound **7** formed an additional hydrogen bond with Lys162, accompanied by the thiazole and keto group of the compound. However it lost the hydrogen bonds shared by other residues during docking. Unlike compound **1** and **7**, compound **9** is capable of preserving the hydrogen bonds shared by the residues Asparagine

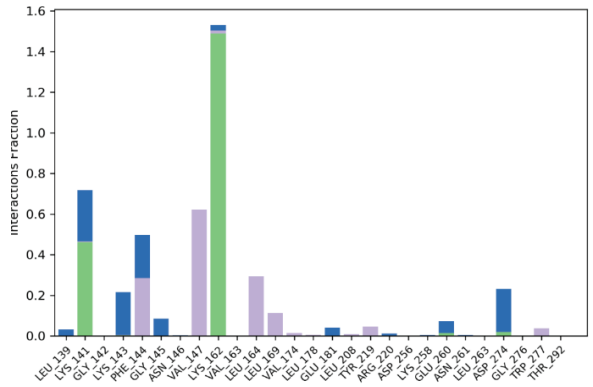

Compound 1

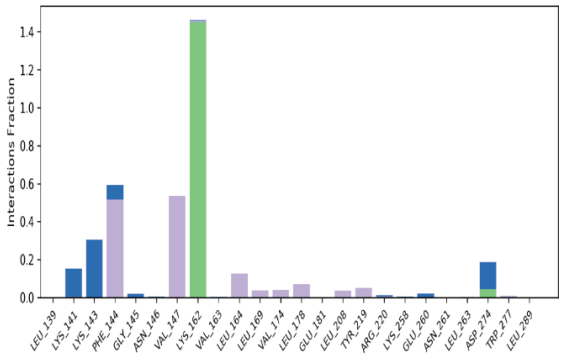

Compound 7

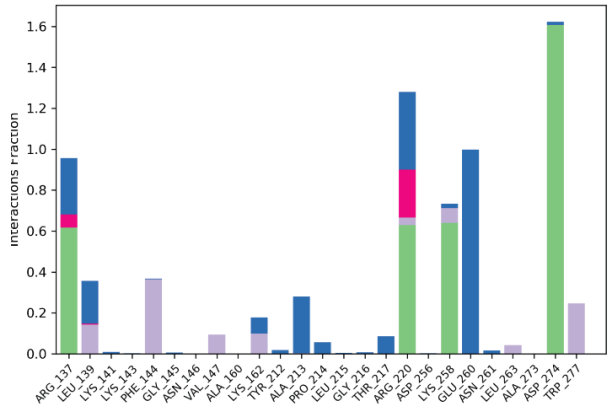

Compound 9

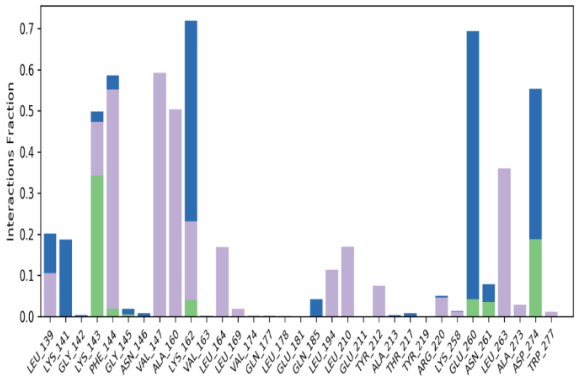

Compound 13

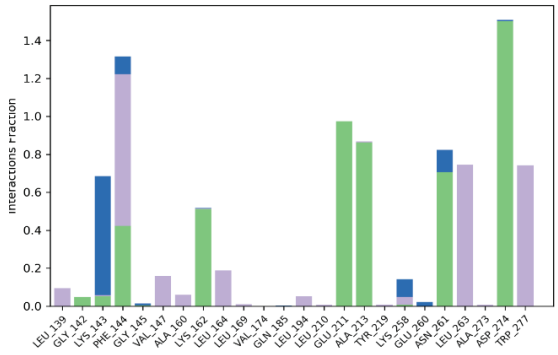

Compound 19

Figure 6. The plot represents the hydrogen bonding interactions of compounds 1, 7, 9, 13, 19 with esteem to deposits of 1MQ4 throughout 100 ns MD simulation.

and arginine. It was also noted that ASP 274 shared two hydrogen bonds with the two N-H groups of the compound, maintaining the same for more than 75% simulation time. To summarize all the above mentioned compounds were found to have good interaction with the active pocket at the kinase domain of aurora kinase, disrupting its action, thereby inhibiting cell growth and induce apoptosis. Overall, it can be concluded that the compounds in particular compound **19**, compound **1**, compound **9** and compound **7** can be used as a potential inhibitor in targeting the enzyme aurora kinase upon experimental validation.

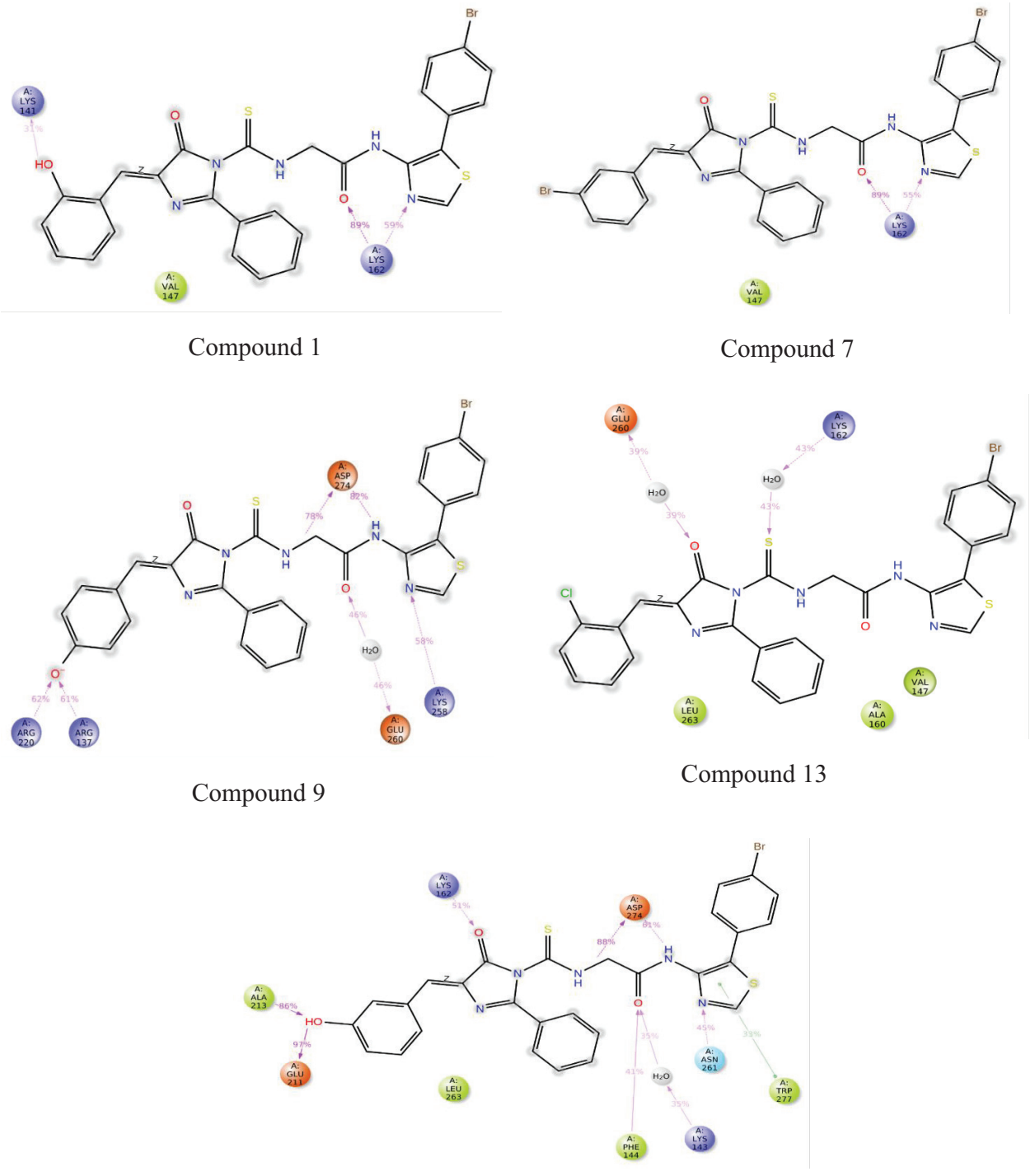

Figure 7. Two-dimensional diagram of Compounds 1, 7, 9, 13, 19 interactions (top) during 100 ns MD simulation and hit molecule compound 19_1MQ4 interaction (bottom).

MM-GBSA free energy studies

Estimation of binding energy using the molecular mechanics-generalized born surface area (MMGBSA) system helps in identification of ligands that bind effectively. The bound complexes identified by molecular docking and MDS were further discovered by performing MMGBSA binding free energy calculations. The key contributors for binding namely Hbonding, lipophilic interactions, electrostatic interactions and Van der Waals energy were also estimated from the trajectories attained throughout MDS and depicted in (Table 3). The allosteric site of the protein Aurora kinase is predicted to be more preferable for the binding of the chosen ligands (Lokhande et al. 2022). The corresponding binding free energies of the compounds are -125.18, -102.40, -96.91, -88.51 and

-84.88 Kcal/mol. for molecules **19, 7, 9, 1** and **13** respectively indicating the binding affinity in the order of Mol**19** > Mol**7** > Mol**9** > Mol**1** > Mol**13**.

Table 3. The binding free energy particulars of the aurora kinase compounds 1, 7, 9, 13, 19 complexes.

Compound	Compound 1	Compound 7	Compound 9	Compound 13	Compound 19
ΔGbind	-88.51	-102.40	-96.91	-84.88	-125.18
ΔGcoloumb	-32.31	-30.07	-43.86	-33.56	-36.72
ΔEHbond	-1.64	-1.97	-3.26	-2.09	-2.96
ΔElipo	-32.96	-40.70	-44.74	-39.01	-50.85
ΔEvdw	7.27	-68.75	-71.36	-73.87	-81.21
Solv GB	41.70	35.99	60.11	39.72	32.36

Conclusions

In this study employed a large-scale computational analysis of 39 compounds with imidazolinone backbones that exhibit inhibitory effects on aurora kinases. The primary objective was to identify the key structural characteristics and properties associated with the biological activity of these compounds against breast cancer, with the ultimate goal of enhancing their potential as successful leads in drug discovery. To achieve this objective, a hybrid strategy combining ligand-based and structure-based methods for drug development was utilized. Notably, the study relied on the properties of a quantitative structure-activity relationship (QSAR) model specifically developed for imidazolidin-4-one derivatives. This approach proved to be straightforward and highly effective in guiding the design of novel imidazolidin-4-one derivatives. The screening process incorporated various techniques, including QSAR, molecular docking, and molecular dynamics simulations. Molecular dynamics simulations were particularly valuable as they provided insights into the stability dynamics of selected compounds (**1, 7, 9, 13** and **19**) within the active site. Over the course of a 100 nanosecond trajectory, the MD simulations demonstrated a high degree of stability for all five examined complexes. Furthermore, the newly designed compounds were evaluated for their inhibitory effects on enzyme activity and other receptors. The results of these assessments, combined with the knowledge gained from the study, suggest that further modifications to the ring system could contribute to the development of lead candidates with significant potential as therapeutic agents for breast cancer treatment.

Declaration of competing interest

The authors declare that there are no competing financial interests.

Funding

No funding was received to assist with the preparation of this manuscript.

Ethical statement

This work does not involve the use of humans or animals

Availability of data and material

All datasets collected and analyzed during this study are available in supplementary information.

Acknowledgments

Authors are grateful to The Management, SRM College of Pharmacy for their consistent support and encouragement.

References

Adawara SN, Shallangwa GA, Mamza PA, Ibrahim A (2020) Molecular docking and QSAR theoretical model for prediction of phthalazinone derivatives as new class of potent dengue virus inhibitors. Beni-Suef University Journal of Basic and Applied Sciences 9: 1–17. https://doi.org/10.1186/s43088-020-00073-9

Behera SK, Vhora N, Contractor D, Shard A, Kumar D, Kalia K, Jain A (2021) Computational drug repurposing study elucidating simultaneous inhibition of entry and replication of novel corona virus by Grazoprevir. Scientific Reports 11: 1–11. https://doi.org/10.1038/s41598-021-86712-2

Chen G, Liu W, Yan B (2022) Breast Cancer MCF-7 Cell Spheroid Culture for Drug Discovery and Development. Journal of cancer therapy 13: 117–130. https://doi.org/10.4236/jct.2022.133009

Chumsri S, Howes T, Bao T, Sabnis G, Brodie A (2011) Aromatase, aromatase inhibitors, and breast cancer. The Journal of Steroid Biochemistry and Molecular Biology 125: 13–22. https://doi.org/10.1016/j.jsbmb.2011.02.001

Gramatica P (2020) Principles of QSAR modeling: comments and suggestions from personal experience. International Journal of Quantitative Structure-Property Relationships (IJQSPR) 5: 61–97. https://doi.org/10.4018/IJQSPR.20200701.oa1

Hehnly H, Canton D, Bucko P, Langeberg LK, Ogier L, Gelman I, Santana LF, Wordeman L, Scott JD (2015) A mitotic kinase scaffold depleted in testicular seminomas impacts spindle orientation in germ line stem cells. Elife 4: e09384. https://doi.org/10.7554/eLife.09384.018

Jia J, Yin H, Chen C, Hu M, Zhong Q, Zheng S, Zhang W, Li H, Xu L, Wang G, He L (2022) Design, synthesis, and evaluation of a novel series of mono-indolylbenzoquinones derivatives for the potential treatment of breast cancer. European journal of medicinal chemistry 237: 114375. https://doi.org/10.1016/j.ejmech.2022.114375

Jung FH, Pasquet G, Lambert-van der Brempt C, Lohmann J-JM, Warin N, Renaud F, Germain H, De Savi C, Roberts N, Johnson T (2006) Discovery of novel and potent thiazoloquinazolines as selective Aurora A and B kinase inhibitors. Journal of medicinal chemistry 49: 955–970. https://doi.org/10.1021/jm050786h

Karahalil B, Yardım-Akaydin S, Nacak Baytas S (2019) An overview of microtubule targeting agents for cancer therapy. Arhiv za higijenu rada i toksikologiju 70: 160–172. https://doi.org/10.2478/aiht-2019-70-3258

Khalifa ME (2021) Design, synthesis and molecular docking study of new purine derivatives as *Aurora* kinase inhibitors. Journal of Molecular Structure 1229: 129843. https://doi.org/10.1016/j.molstruc.2020.129843

Khetmalis YM, Chitti S, Wunnava AU, Kumar BK, Kumar MM.K, Murugesan S, Sekhar KVGC (2022) Design, synthesis and anti-mycobacterial evaluation of imidazo [1, 2-a] pyridine analogues. RSC Medicinal Chemistry 13: 327–342. https://doi.org/10.1039/D1MD00367D

Leino TO, Sieger P, Yli-Kauhaluoma J, Wallén EA, Kley JT (2022) The azulene scaffold from a medicinal chemist's perspective: Physicochemical and in vitro parameters relevant for drug discovery. European Journal of Medicinal Chemistry 237: 114374. https://doi.org/10.1016/j.ejmech.2022.114374

Lokhande KB, Ballav S, Yadav RS, Swamy KV, Basu S (2022) Probing intermolecular interactions and binding stability of kaempferol, quercetin and resveratrol derivatives with PPAR-γ: docking, molecular dynamics and MM/GBSA approach to reveal potent PPAR-γ agonist against cancer. Journal of Biomolecular Structure and Dynamics 40: 971–981. https://doi.org/10.1080/07391102.2020.1820380

McEwan S (2021) Disrupting inhibitory-kappaB kinase (IKK)-*Aurora* kinase signalling in prostate cancer cells.

Rosário-Ferreira N, Baptista SJ, Barreto CA, Rodrigues FE, Silva TF, Ferreira SG, Vitorino JN, Melo R, Victor BL, Machuqueiro M (2021) *In Silico* endto-end protein–ligand interaction characterization pipeline: The case of SARS-CoV2. ACS Synthetic Biology 10: 3209–3235. https://doi.org/10.1021/acssynbio.1c00368

Siegel RL, Miller KD, Fuchs HE, Jemal A (2022) Cancer statistics, 2022. CA: A cancer journal for clinicians 72: 7–33. https://doi.org/10.3322/caac.21708

Siva Kumar B, Anuragh S, Kammala AK, Ilango K (2022) Computer aided drug design approach to screen Phytoconstituents of Adhatoda vasica as potential inhibitors of SARS-CoV-2 Main protease enzyme. Life 12: 315. https://doi.org/10.3390/life12020315

WHO [Organization, W.H.] (2022) BioHub system: progress report [May 2022].

Supplementary material 1

Supplementary data

Authors: Bathula Sivakumar, Ilango Kaliappan

Data type: docx

Link: https://doi.org/10.3897/pharmacia.70.e114935.suppl1